EPJ Web of Conferences **184**, 01015 (2018) https://doi.org/10.1051/epjconf/201818401015
9th European Summer School on Experimental Nuclear Astrophysics

Gas detectors for nuclear physics experiments

Dimitra Pierroutsakou[1,⋆]

[1] *INFN - Sezione di Napoli, Via Cintia, I-80126 Napoli, Italy*

Abstract. In this lecture I will present the operation principle and the different kinds of gas detecting systems for charged particles employed in high-energy and low-energy physics environments, with particular focus on the requirements of nuclear physics experiments with low-energy Radioactive Ion Beams (RIBs). I will show in more details an example of gas detector used at the RIB in-flight facility EXOTIC, for the ion beam tracking and for time of flight measurements. Finally, I will discuss the use of an active target in nuclear physics experiments with RIBs together with some key improvements of first generation devices required for facing the challenges of more intense RIBs.

1 Operation principle and different kinds of gas detectors

Gas detectors are planned or being constructed at every nuclear physics facility because they have some important advantages with respect to solid state devices for charged particle detection. To summarize their characteristics, they have: a) good stability, robustness and aging compared to solid state detectors; b) high radiation length; c) possibility to tune the effective thickness; d) low energy thresholds; e) three dimensional readout/flexible geometry; f) good space and moderate energy resolution; g) medium rates for particles. Finally, for large-area coverage with low material budget they are still the only solution.

Their **operation principle** is based on the ionization and excitation of the gas molecules caused by the passage of the charged particle. Electron-ion pairs are created either from the particle itself or by δ-rays and the average energy necessary to create one ion-pair, about W=25-30 eV, is not much dependent on the gas. Some non-ionizing energy loss (excitation) makes the number of pairs lower and this is important for the detector energy resolution. The number N of produced pairs follows a Poisson distribution $\sigma = \sqrt{N}$. Without electric field, electron-ion pairs diffuse due to random thermal movement and suffer collisions with gas molecules. In these collisions, recombination of ions to neutrals (for molecular ions), electron attachment in gases with large electron affinity and charge exchange can occur. In case of diffusion of electron-ion pairs in electric field, when high voltage (HV) is applied to the electrodes of the detector, we have the superposition of thermal velocity (random) and drift velocity of electrons/ions along the lines of the electric field. Electrons are much faster than positive ions, by a factor of about 1000. A magnetic field parallel to the electric field will curl up electrons in the transverse (to the direction of motion) plane reducing their transverse diffusion.

By increasing the HV and according to the multiplication of the primary number of created electron-ion pairs (gain), the detector can operate in different regimes: **a**) **Ionization mode** with full charge collection and no multiplication, gain ≈ 1; **b**) **Proportional mode** with multiplication of the

⋆e-mail: pierroutsakou@na.infn.it

primary ionization, a signal that is proportional to the ionization, possibility to measure dE/dx, where secondary avalanches need quenching (quenching gas is a neutral gas with a lower ionization potential, added to the main detector gas that quenches the ion multiplication by neutralizing ions of the main chamber gas), gain $\approx 10^4$-10^5; **c**) **Limited proportional mode** where the created space charge distorts the electric field, we have loss of proportionality and strong photoemission that requires strong quenchers or pulsed HV, gain $\approx 10^8$; **d**) **Geiger mode** with a signal amplitude independent of energy, massive photoemission, where the full length of the anode wire is affected and the discharge can be stopped by HV cut, gain $> 10^8$.

A detector that works in the first regime is the **ionization chamber**. It consists of two metallic electrodes at distance d covering a volume gas and the application of a HV to the electrodes creates a constant electric field.

In the **proportional counter** (proportional regime) that has a single anode wire in a cylindrical cathode, the created electric field $E \sim \frac{1}{r}$ is very strong near the anode wire and weak for larger distances r. The electron-ion pairs created from the passage of a particle drift in the volume while multiplication of the primary charge occurs only near the anode wire through an avalanche process. Many closely spaced anode wires in the same chamber can each act as an independent proportional counter. This is the **Multiwire Proportional Counter** (**MWPC**) invented by G. Charpak, CERN 1968, Nobel Prize 1992. The basic configuration of a MWPC is two cathode planes and a wire anode in between. It has many advantages: a very flexible geometry and a large detection area ($\approx$ m^2); possibility to work in magnetic field, with a rate capability $\approx 10^4$ Hz/mm^2; gain $\approx 10^4$-10^5; possibility to perform Particle IDentification (PID) through dE/dx measurement and many well developed position encoding methods: binary readout (identification of the closest anode wire to the avalanche), charge division by using resistive anode wires and analogue readout of the signals of a segmented cathode. By using several layers of MPWC giving x-y position it is possible to perform tracking of the charged particle.

A variant of the MWPC is the **Parallel Plate Avalanche Counter** (**PPAC**), preferred when fast timing is more important than energy resolution. The basic configuration of a PPAC is two planar electrodes covering a gas at low pressure, P=7-20 mbar, that yields a uniform intense reduced electric field $\frac{E}{P}$. The avalanche multiplication starts immediately from the primary ionization electrons resulting in a very good time resolution (of the order of hundred of ps for 1 mm gap) and a high counting rate capability. However, a larger amplification of the primary ionization occurs near the cathode resulting in a dependence of the signal on the position of the ionizing event and consequently, in a poor energy resolution ($\sim$20%). A hybrid configuration of the detector is MWPC + PPAC or position-sensitive PPAC. The wire structrure of the position-sensitive PPAC gives position information, while it introduces a second step of multiplication near the wires.

Although wire-based detectors have been extensively used in both high-energy and low-energy physics experiments, they present some drawbacks: a) gain limits; b) counting rate limits (space charge); c) aging after long-term operation. The need for gas detectors that could operate at high counting rates led to the development of **micro − strip gas chambers** (**MSGCs**) [1]. Operation at high counting rate was achieved by increasing the granularity of the anode and by adding cathodes very close to the anodes to evacuate ions during the avalanche process. The electrodes are formed on insulating substrate by micro-lithographic technology. However, MSGCs proved difficult to operate in challenging conditions and were prone to aging and sparking. The invention of the **Micropattern gas detector** (**MPGD**), such as the micromesh gaseous structure chamber (the MicroMegas) [2] and the gas-electron multiplier (GEM) detector [3], appears to have solved these problems. MPGDs have small avalanche gaps and therefore a rapid signal development, implemented in slightly different ways. In MicroMegas detectors the electron multiplication takes place in the narrow gap between a thin cathode mesh with holes and the anode. GEMs, on the other hand, have a

thin metal-coated polymer (Kapton) foil chemically produced with a high density of holes and the multiplication takes place in the holes in the foil.

The **drift chamber** gives spatial information by measuring the electrons drift time. The time measurement starts by an external (fast) detector, i.e. scintillator counter. The electrons drift to the anode (sense wire) in the field created by the cathodes and their arrival at the anode stops the time measurement. The spatial resolution of the drift chamber depends on: a) the electron diffusion and, thus, on the drift path and b) the time resolution of the electronics, including the start detector.

A combination of MWPC and drift chamber is the **Time Projection chamber** (**TPC**). Its geometry is mostly cylindrical with a central HV cathode, a MWPC at one end-cap of the cylinder and with a magnetic field B parallel to the electric field E. The electrons drift to the end-caps in homogeneous E. The drift distance is of several meters and the amplification of the primary ionization occurs at the end of the drift. With the TPC it is possible to perform a full 3D reconstruction of the particle trajectory, xy coordinates are obtained from the anode wires and cathode pads of MWPC and z is deduced from the drift time measurement. A PID is also possible by measuring the momentum via dE/dx.

For further reading relative to this section, the reader can also refer to [4–9].

2 Gas detectors in nuclear physics experiments with RIBs

In low-energy nuclear physics experiments with RIBs some key features should be taken into consideration for the design of detecting systems: the beams produced by first generation facilities have low intensity (up to 10^7 pps), large energy spread and large emittance (in-flight production) and sometimes a high background. To face these problems the detection system should be highly efficient, with good energy and angle resolution, low energy threshold, able to suppress background (by performing coincidence measurements), to perform event-by-event ion beam tracking and a full kinematic reconstruction. To achieve high statistics, the target should be thick enough, though a thick target results in a poor energy resolution.

Figure 1. (color online) Left panel: Schematic exploded view of the position-sensitive PPACs electrodes. Middle panel: Electrode package. Right panel: Final assembly of the position-sensitive PPAC.

In the following I present the position-sensitive PPACs employed for nuclear physics and nuclear astrophysics experiments with the low-energy RIBs delivered by the in-flight facility EXOTIC (Legnaro National Laboratory of INFN, Italy) [10–13]. The two position-sensitive PPACs are dedicated to the RIB tracking system and to Time of Flight (ToF) measurements. They are placed upstream the reaction target that is installed at the focal plane of the EXOTIC facility. For more details on the experimental set up of the facility see [14]. They have a three-electrode structure (Figure 1, left-hand side): a central cathode and two anodes, placed symmetrically with respect to the cathode at a distance of 2.4 mm. The detector active area is 62 x 62 mm^2. The cathode is made of a 1.5 μm-thick stretched mylar foil with 30 nm of aluminum evaporated on both surfaces. Each anode is a mesh of 60 20 μm-thick wires in the x and y directions, with a spacing of 1 mm. The wires of the first anode

are oriented horizontally and those of the second one vertically. The position information of a particle crossing the PPAC is extracted from the anode signals by using a delay-line readout. Each wire is electrically connected to discrete LC circuit delay lines of 2.3 ns/mm each, with a 50 Ω impedance, resulting in a total delay of 138 ns in both the x and the y direction. The cathode signal is used as a reference time for ToF measurements and for trigger purposes. The PPAC is filled with C_4H_{10} (high gain at low pressure) at a working pressure of 10-20 mbar. The cathode is biased at a negative potential of 550-970 V while the anodes are kept at ground potential. In this way, reduced electric fields of 200-230 V/cm/mbar are obtained.

A very important issue for handling the PPAC signals, in order to have a good position resolution and a high tracking efficiency, is the noise reduction that can be reached by performing a careful grounding and by using a low-noise fast preamplifier, placed very close to the PPAC. The cathode signal and the anode signals x_1, x_2, y_1, y_2, extracted from each end of the delay lines are sent to this fast preamplifier, followed by a further amplification in a fast amplifier and then is sent to a Constant Fraction Discriminator (CFD) to set a threshold and extract logic signals (left-hand side of Figure 2). Finally, it is a sent to a Time to Digital Converter (TDC). The position determination of the detected particle is achieved by measuring with a TDC the time interval, t_{x1}, t_{x2}, t_{y1} and t_{y2}, between a common start (given by the master trigger signal) and the delay line outputs. The positions of a particle crossing the PPAC are: $X_{position} = k\ (t_{x1} - t_{x2})/2\ (mm)$ and $Y_{position} = k\ (t_{y1} - t_{y2})/2\ (mm)$, where $k = 0.435$ mm/ns is the slope for the x and y delay lines. The good events retained in the analysis are those lying on the diagonal of the $(t_{x2} - t_K)$ *vs* $(t_{x1} - t_K)$ correlation plot (shown on the right-hand side of Figure 2) that satisfy the equation: *total delay line* $= (t_{x1} - t_K) + (t_{x2} - t_K)$, with t_K the time interval between the common start and the cathode signal. Selecting these events allows us to reject pile up events and multiple hit events.

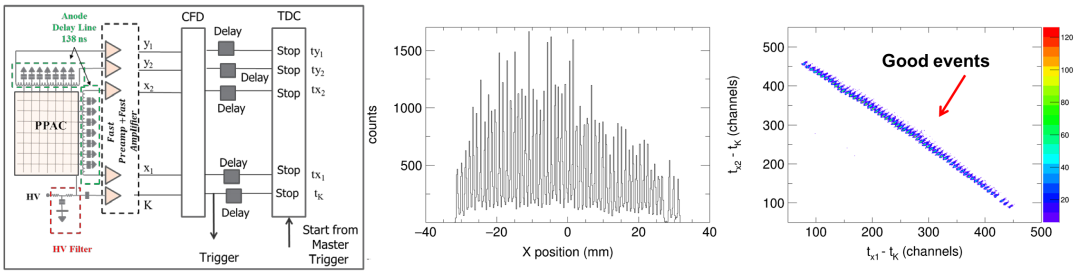

Figure 2. (color online) Left-hand side: Electronics of a position-sensitive PPAC. X position (middle) and $(t_{x2} - t_K)$ *vs* $(t_{x1} - t_K)$ correlation plot (right-hand side) obtained for an ^{241}Am α source. For details see text.

The PPAC has 0.86 ns FWHM time (intrinsic) resolution, allowing ToF measurements between PPAC and the silicon detectors of the EXPADES array [14] with a FWHM overall time resolution of about 1.5 ns. Furthermore, the 0.7 mm FWHM position resolution of the PPACs (binary readout, FWHM $=2.35\frac{1}{\sqrt{12}}\ mm$) permits reconstruction of the event position on the reaction target with 1.6 mm FWHM resolution. The PPACs were found to be able to sustain high counting rates up to $\sim 10^6$ Hz and to have a tracking efficiency of 90%-98%, depending on the charge (Z=3-9) and the rate of the produced RIB.

3 Active chamber for experiments with low-energy RIBs

In nuclear physics experiments with low-energy RIBs the use of an active target, a device that acts as target and as detector (TPC) simultaneously, presents potentially some interesting features: 4π

geometry; full 3D tracking of all particles (from position resolution is deduced the energy resolution at the vertex); allows to use high thickness of the target without loss of energy resolution (gain up to 100); low energy threshold; possibility to detect also unbound states; very low background in many cases (coincident measurements); excitation function can be done in a single measurement (important for resonant experiments: quasi-molecular structures and experiments of astrophysical interest); versatility.

One of the first generation active targets, MAYA [16], can be seen on the left-hand side of Figure 3. In this device the projected trajectories on the cathode pads (1024 pads) of the charged particles are used to have a 2D image while the third dimension is taken from the electron drift time obtained from the anode wires (32 wires with 2.3-mm gap). The deduced information is angle, energy (from the range or the charge signal) and PID (through the correlation plot range *vs* charge). A wall of ancillary detectors (Si+CsI) at the exit of MAYA are used for the detection of particles that go through. The amplification gain is 10^3-10^4 and the RMS position resolution $\sim$ 1 mm for a pad pitch 0.9 cm. The position resolution determines the angular and range resolution and thus, it determines the energy resolution and the PID for stopped particles. For particles that go through, the PID is obtained via ΔE-E technique.

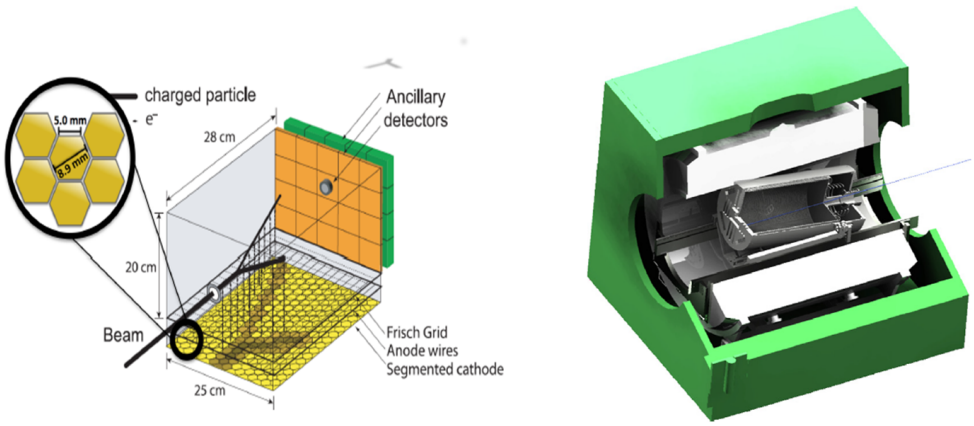

Figure 3. (color online) Left-hand side: MAYA [16]. Right-hand side: AT-TPC [17].

There are some limits in such a first generation active target: poor dynamic range $\sim$ 20; can sustain a limited rate due to the electronics high dead time > 2 ms; position resolution since it is hard to reconstruct trajectories for ranges of few cm. Finally, only two-body reactions can be considered because the drift time deduced from wires does not allow dealing with multi-hit events.

For more intense RIBs (provided by facilities like SPES, SPIRAL2, ISOLDE etc), second generation active targets are required to overcome the above described limitations. Switching from wire-based amplification to amplification based on MPGDs renders second generation devices robust, eliminates ion backflow permitting large range of beam rates, allows high rate and high dynamic range, dealing with multi-hit events, better position resolution, better PID, larger target thickness (from 25 to 100 cm), more versatility. The trigger can be both internal and external. The use of GET (General electronics per TPCs) allows to handle up to 30000 channels.

Various second generation active targets have been already built or are under construction (for a detailed list see [17]). Here, I just refer to ACTAR (in construction, funded by ERC Starting Grant, G.F. Grinyer) and AT-TPC in construction at NSCL (FRIB, USA) [17]. ACTAR is cubic or cuboid with about 16000 channels and amplification of MicroMegas-type. It uses GET electronics and auxiliary particle detectors are employed for the detection of charged particles that go through (Si+Si or Si+CsI) and for γ rays ($LaBr_3$ or $CeBr_3$). AT-TPC (see right-hand side of Figure 3) is a cylinder (l=1 m, ϕ=55 cm for an active volume of 250 l) inside a 2T solenoid. This allows the measurement of the particle momentum from the curvature giving a better energy resolution compared with that deduced from the particle range and, moreover, it allows the characterization of energetic particles leaving the volume. There is no need for ancillary detectors and the trigger is internal. The employed magnetic field increases the range to stop the particles and focuses drift electrons yielding in a better localization. The amplification is also in this case of MicroMegas type. The axis of the detector is tilted by 7° to spread tracks for small angles permitting pile up reduction by a factor about 500.

4 Summary

I presented the operation principle and different gas detecting systems, focusing on the requirements of nuclear physics experiments with low-energy RIBs. An example of gas detector, operating at the in-flight RIB facility EXOTIC was described: position-sensitive PPAC for the RIB tracking and for ToF measurements. Moreover, an interesting device for nuclear physics experiments with RIBs was discussed: the active target. Both first and second generation active targets were presented, describing the achieved improvements for addressing challenges with more intense RIBs, delivered from second generation facilities.

References

[1] A. Oed, NIMA **263** (1988) 351
[2] Y. Giomataris et al. NIM A **376** (1996) 29
[3] F. Sauli, NIMA **386** (1997) 531
[4] "Techniques for nuclear and particle physics experiments", W. R. Leo
[5] "Radiation Detection And Measurement", G. Knoll
[6] "Tracking Detectors", Lecture, N. Wermes, SLAC Summer Institute 2016 "New Orizons on the energy frontier"
[7] "Gaseous detectors for radioactive beam experiments", D. Suzuki and "Trend and new developments in gas amplifiers: a concise review", M. Cortesi, GDS Topical Meeting: GDS coupling to auxiliary detection systems, January 25-27, 2017 INFN Laboratori Nazionali di Legnaro
[8] "Making radioactive ion beams - Detecting reaction products ", R. Raabe, Rewriting Nuclear Physics Textbooks 30 years with Radioactive Ion Beams Physics, Pisa, July 2015
[9] F. Sauli, Physics Reports 403–404 (2004) 471–504
[10] V.Z. Maidikov et al., Nucl. Phys. A **746** (2004) 389c
[11] D. Pierroutsakou et al., Eur. Phys. J. Special Topics **150** (2007) 47
[12] F. Farinon et al., Nucl. Instr. and Meth. B **266** (2008) 4097
[13] M. Mazzocco et al., Nucl. Instr. and Meth. B **266** (2008) 4665; Nucl. Instr. and Meth. B **317** (2013) 223
[14] D. Pierroutsakou et al., Nucl. Instr. and Meth. A **834** (2016) 46
[15] D. Guillemaud-Mueller et al., IEEE Trans. Nucl. Sci. **33** (1) (1986) 343
[16] C.E. Demonchy et al., Nucl. Instr. Meth. A **583** (2007) 341
[17] S. Beceiro-Novo, T. Ahn, D. Bazin, W. Mittig, Progr. Part. and Nucl. Phys. **84** (2015) 124–165